

Cerium Regulating Ru-O Covalency Enhance RuO₂ Acidic Oxygen Evolution Reaction

Pingping Wang^{a ‡}, Jinglin Mu^{a ‡}, Guozhou Feng^a, Yuxin Fan^a, Yaping Pan^b, Lechen
Diao^{a *}, Zhichao Miao^a, Jin Zhou^{a *}

^a School of Chemistry and Chemical Engineering, Shandong University of Technology,
Zibo 255000, PR China

^b State Key Laboratory for Physical Chemistry of Solid Surfaces, Collaborative
Innovation Center of Chemistry for Energy Materials, and College of Chemistry and
Chemical Engineering, Xiamen University, Xiamen 361005, China

[‡] These authors contributed equally to this work.

^{*} Co-corresponding author.

E-mail address: diaolechen@sdut.edu.cn (Lechen Diao), zhoujin@sdut.edu.cn (Jin
Zhou)

1. Experimental section

1.1 Materials Synthesis

All the chemicals are analytical grade obtained from commercial suppliers and are used directly without further purification. Ruthenium (III) chloride ($\text{RuCl}_3 \cdot x\text{H}_2\text{O}$), cerium nitrate hexahydrate ($\text{Ce}(\text{NO}_3)_2 \cdot 6\text{H}_2\text{O}$, 99%), potassium hydroxide (KOH) were purchased from Shanghai Aladdin Biochemical Technology. Nafion (5 wt%) was purchased from Sigma Aldrich Chemical Reagents. Sulfuric acid was purchased from Chongqing Chuandong Chemical. Carbon paper purchased from Wuhu Owl Material Technology.

1.1.1 Synthesis of N-CN

1.25g glucose and 25g sodium chloride were dissolved in 75 mL deionized water. The mixed solution was poured into a petri dish and freeze-dried under vacuum at -50°C . The obtained white composite powder was mixed with urea (1.25 g). Then, the above precursor was annealed at 650°C for 2 hours in a flowing N_2 atmosphere (100 mL min^{-1}) with a heating rate of $10^\circ\text{C min}^{-1}$. The products were washed with deionized water and then lyophilized at -50°C for 24 h.

1.1.2 $\text{Ce}_x\text{Ru}_{1-x}\text{O}_2$ synthesis

a certain proportion of $\text{RuCl}_3 \cdot x\text{H}_2\text{O}$ and $\text{Ce}(\text{NO}_3)_2 \cdot 6\text{H}_2\text{O}$ (total 1.25 g) were dissolved in 20 mL of deionized water. The prepared N-CN (0.30 g) was dispersed in the prepared salt solution by ultrasonic dispersion for 30 min and stirring for another 12h in 35°C . The N-CN with metal ion on its surface was filtered and washed by deionized water. Then, the obtained composite material was calcined in a muffle furnace at 500°C with a ramp rate of 2°C min^{-1} . The molar ratio of Ce and Ru in the resulting products were tested by Inductively coupled plasma optical emission spectrometry (ICP-OES). According to the above result, the products were named as RuO_2 , $\text{Ru}_{0.01}\text{Ce}_{0.99}\text{O}_2$, $\text{Ru}_{0.05}\text{Ce}_{0.95}\text{O}_2$.and $\text{Ru}_{0.10}\text{Ce}_{0.90}\text{O}_2$

1.2 Materials Characterization

The microstructure of the materials was characterized by scanning electron microscopy (SEM, FEI Thermo) and transmission electron microscopy (TEM, Tecnai G2 F20). The phase structure was analyzed by X-ray powder diffraction (XRD, Bruker)

with Cu K α radiation (40 kV, 30 mA,) at a rate of 10° min⁻¹. X-ray photoelectron spectroscopy (XPS) data were recorded on Escalab 250Xi and analyzed by XPS Peak software. ICP-OES results were collected with the Agilent 5110 ICP-OES. Raman tests were carried out on LabRAM HR Evolution.

1.3 Electrochemical Measurement

The electrocatalyst ink was prepared by dispersing 5 mg catalyst materials in the mixed solution of 475 μ L N,N-dimethylformamide and 25 μ L Nafion (5 wt%). The solution was ultrasonic treated for 1h to form a well-dispersed ink, and then dropped on the L-shaped glass carbon electrode with a mass loading of 0.8 mg cm⁻².

All electrochemical measurements were performed in a standard three-electrode system on the CHI760E electrochemical workstation. The L-shaped glass carbon electrode (diameter 3.0 mm) worked as the working electrode and was polished by Al₂O₃ powder before being used. Graphite rod and platinum sheet were used for the opposite electrodes of HER and OER respectively. The reference electrode was Ag/AgCl electrodes (saturated KCl). All the measured potentials were converted to reversible hydrogen electrode potentials calculated as follows: $E_{RHE} = E_{Ag/AgCl} + 0.059 \cdot pH + E_{Ag/AgCl}$.

Linear sweep voltammetry (LSV) tests were performed at a scan rate of 5 mV s⁻¹ in the range of 0.9-1.5V in 0.5 M H₂SO₄. All the LSV curves were corrected with ohmic potential drop (iR) of the solution resistance ($E = E_{RHE} - iR$). In acidic medium, scans were performed at 100 mV s⁻¹ rate, 1000 and 10000 cycle tests were performed in the potential range of 1.2 V-1.4 V vs. RHE, and then LSV was measured to study the long-term cycling stability. The double layer capacitance (C_{dl}) value is measured by cyclic voltammetry tests at different scan rates (20 mV s⁻¹~100 mV s⁻¹) cycling in non-faradic reaction range. Electrochemical impedance spectroscopy (EIS) measurements were performed at the open circuit potential from 10 kHz to 0.1 Hz. The durability test was performed by i-t test at a constant current density of 10 mA cm⁻². Tafel slope plots were calculated by Tafel equation: $\eta = b \times \log j + a$, where η is overpotential, b is Tafel slope, j is current density, and a is constant.

1.4 In situ ATR-SEIRAS tests

In situ ATR-SEIRAS tests were performed in a standard three-electrode system. Au-coated Si pillar with $\text{Ce}_{0.05}\text{Ru}_{0.95}\text{O}_2$ catalysts coating were used as working electrode, while a platinum wire and an Ag/AgCl were used as the counter and reference electrodes, respectively. The background spectrum was first obtained at 1.2 V before the test. Then, the potential was applied to the working electrode ranged from 1.2 to 1.7 V. At the same time, infrared spectra were acquired with a time resolution of 48 seconds per spectrum at a spectral resolution of 8 cm^{-1} .

1.5 DFT calculation

All first-principles calculations were performed using Materials Studio DMol³ version 2019[1, 2]. Configuration optimizations were conducted with the double numeric with polarization basis set, employing the PBE[3] generalized gradient approximation functional, with a force convergence criterion of 0.002 Hartree/\AA . Based on experimental results, the (110) crystal facet was selected for investigation. The slab model used in the calculations consisted of 32 Ru atoms and 64 O atoms, with a vacuum layer thickness of 15 \AA . Ce atom doping at different sites on this slab model and the adsorption of reaction intermediates were studied. The free energies of the reaction steps were determined by the equation: $\Delta G = \Delta E_{\text{ads}} + \Delta \text{ZPE} - T\Delta S$, where ΔE_{ads} represents the adsorption energy of intermediates, and T denotes the temperature. ΔZPE and ΔS correspond to the variations in zero-point energy and entropy, respectively, consistent with values reported in the literature[4]. The final electrode potential was derived from the computational hydrogen electrode[5].

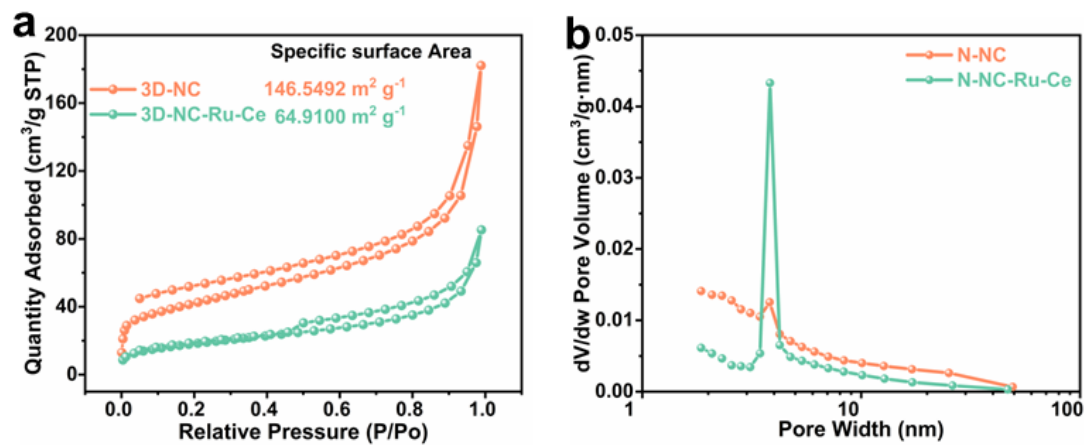


Figure S1 (a) The isothermal adsorption-desorption curves and (b) pore size distribution of 3D-NC and 3D-NC-Ru-Ce.

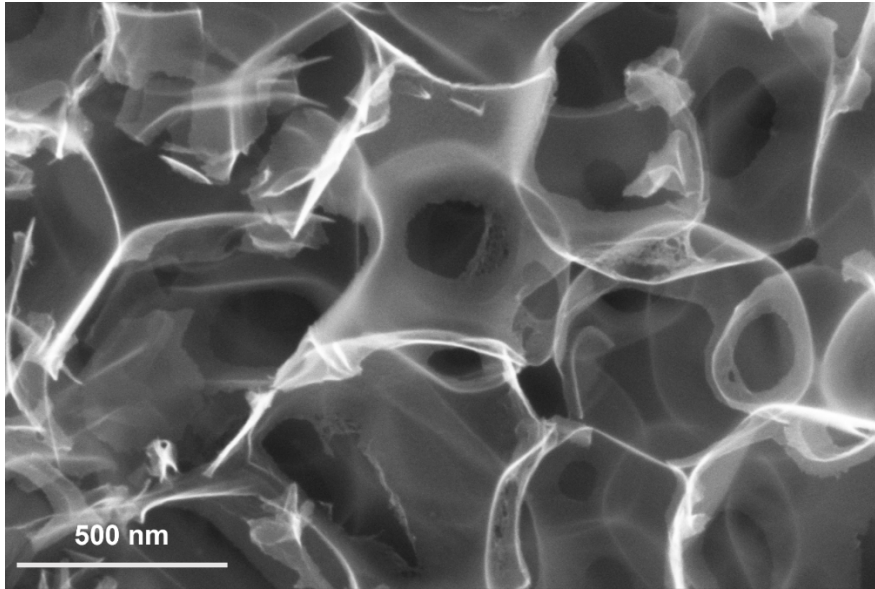


Figure S2 The SEM image of 3D-NC-Ru-Ce.

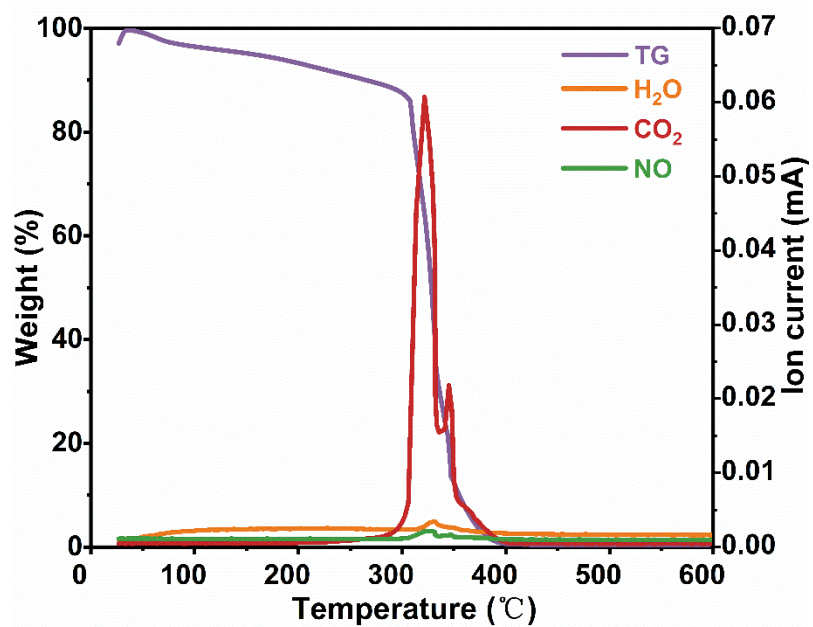


Figure S3. TG-MS curves of 3D-NC-Ru-Ce

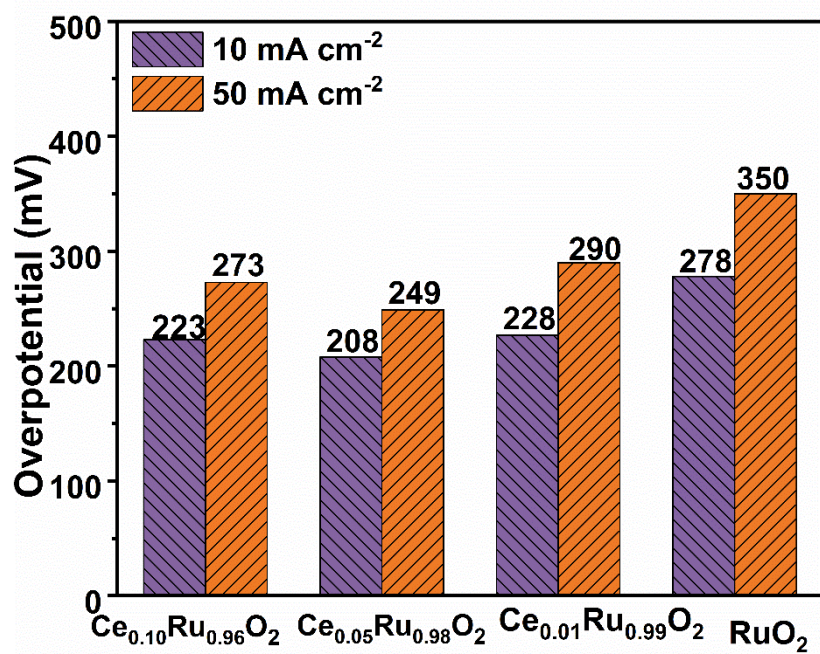


Figure S4 Overpotential of the Ce_xRu_{1-x}O₂ samples at 10 and 50 mA cm⁻².

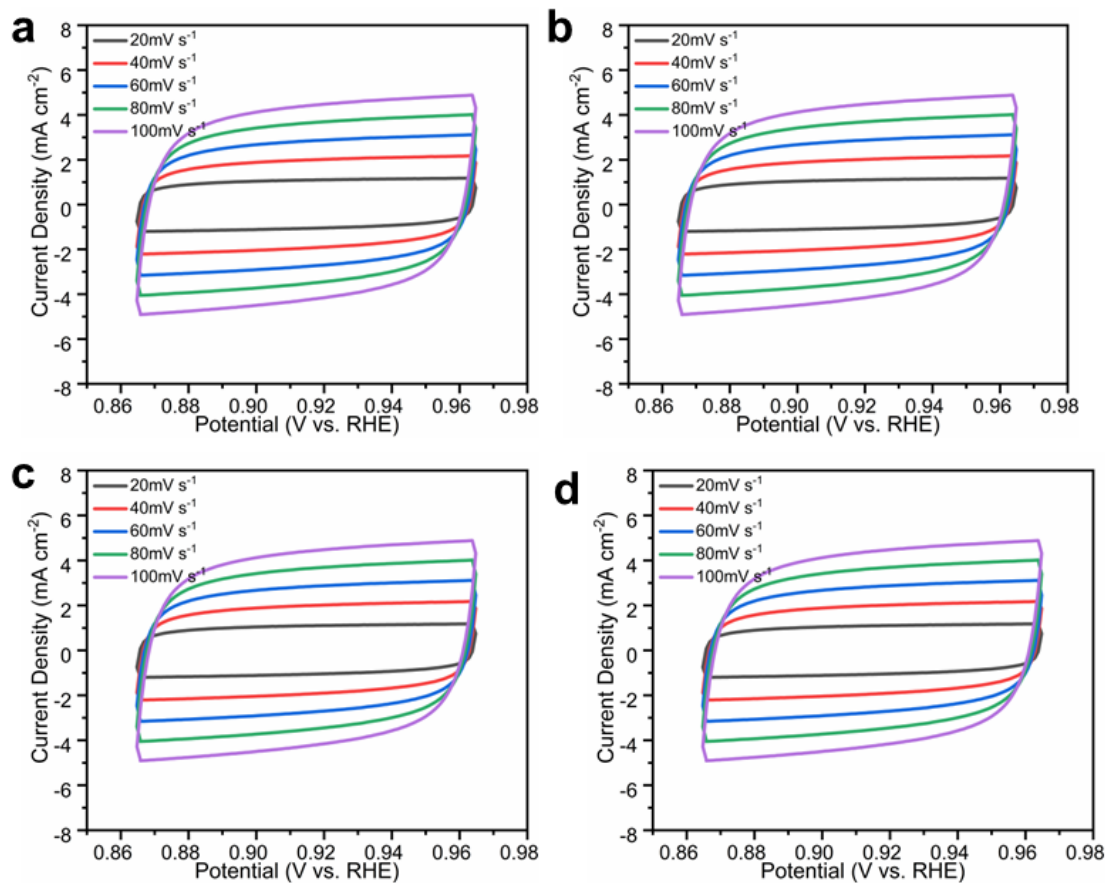


Figure S5 Electrochemical double-layer capacitance measurements. CVs at different sweeping rates from 20 mV s⁻¹ to 100 mV s⁻¹ of (a) Ce_{0.10}Ru_{0.90}O₂, (b) Ce_{0.05}Ru_{0.95}O₂, (c) Ce_{0.01}Ru_{0.99}O₂ and (d) RuO₂.

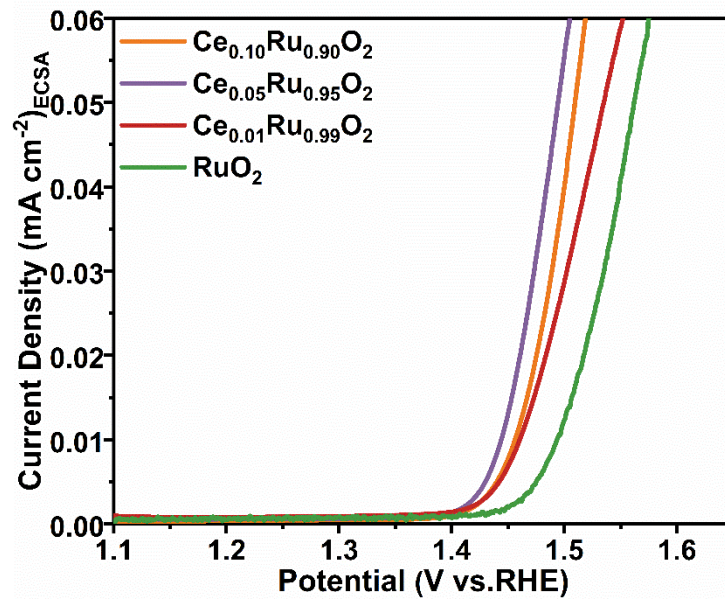


Figure S6 LSV curves of the current density normalized by ECSA.

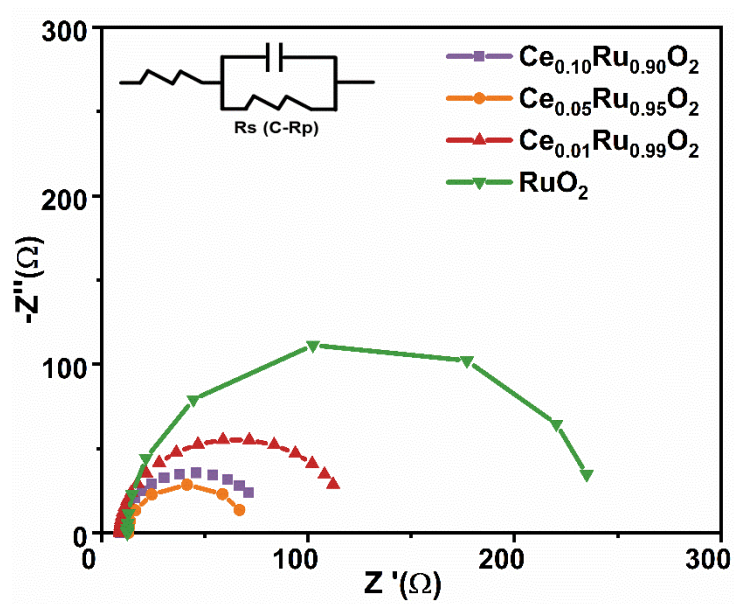


Figure S7 EIS spectra of the samples in 0.5 M H₂SO₄.

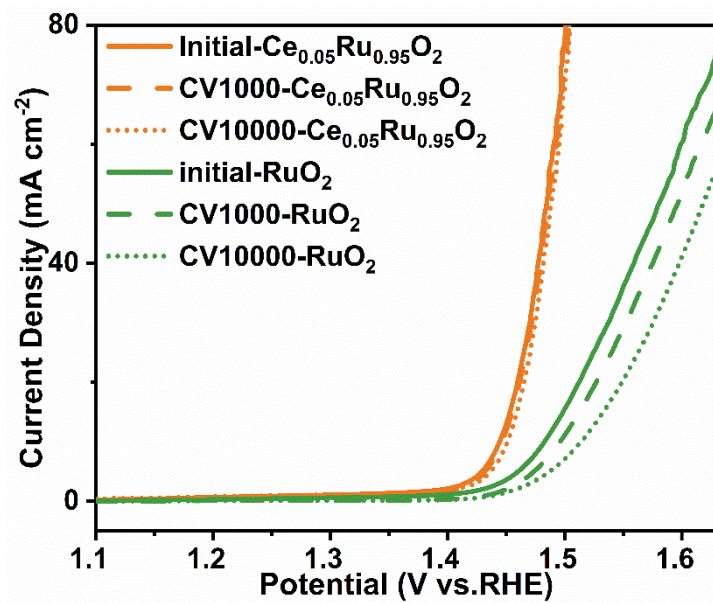


Figure S8 LSV curves of the samples before and after 1000, 10,000 CV tests in 0.5 m H₂SO₄.

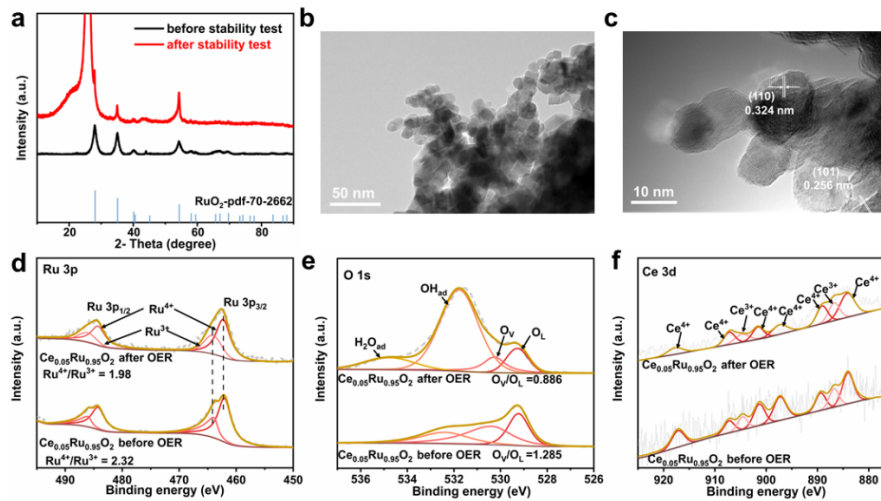


Figure S9 $\text{Ce}_{0.05}\text{Ru}_{0.95}\text{O}_2$ catalyst characterization after stability test. (a) XRD, (b-c) HRTEM, (d) Ru 3p, (e) O 1s, (f) Ce 3d XPS fine spectrum

To better illustrate the enhanced stability of synthesized $\text{Ce}_{0.05}\text{Ru}_{0.95}\text{O}_2$, the XRD, TEM, and XPS characterization were further performed after the stability test (Figure S9). As shown in Figure S9a, catalyst exhibits identical diffraction peak sites in its XRD plot. The HRTEM figure shows that $\text{Ce}_{0.05}\text{Ru}_{0.95}\text{O}_2$ is composed of some nanoparticles approximately 10 nm, and the lattice distances of 0.324 nm and 0.256 nm corresponding to the (110) and (101) planes are consistent with those before stability test. To demonstrate the over-oxidation resistance of $\text{Ce}_{0.05}\text{Ru}_{0.95}\text{O}_2$, XPS fine spectrums of Ru, O, and Ce were analyzed before and after OER (Figure S9d-f). The decreased $\text{Ru}^{4+}/\text{Ru}^{3+}$ ratio after stability test illustrated that Ce atoms donate electrons to Ru sites in the Ru-O-Ce structure to prevent Ru from over oxidation. The O 1s (Figure S9e) spectra shows that the O_v/O_L ratio was obviously decreased after OER. While no obvious difference was observed for Ce 3d between the spectrums before and after stability. These observations illustrate the enhanced stability of synthesized $\text{Ce}_{0.05}\text{Ru}_{0.95}\text{O}_2$.

Table S1. ICP-MS results of $\text{Ce}_x\text{Ru}_{1-x}\text{O}_2$

| | Ce (%) | Ru (%) |
|--|--------|--------|
| $\text{Ce}_{0.01}\text{Ru}_{0.99}\text{O}_2$ | 0.26 | 24.48 |
| $\text{Ce}_{0.05}\text{Ru}_{0.95}\text{O}_2$ | 0.74 | 15.14 |
| $\text{Ce}_{0.10}\text{Ru}_{0.90}\text{O}_2$ | 2.06 | 17.93 |

Table S2. Acid OER overpotential in recent reported literature.

| Catalyst | Overpotential (mV) | Current density (mA cm ⁻²) | ref |
|--|--------------------|--|------|
| C-RuO ₂ -RuSe | 212 | 50 | [6] |
| Ru/Co-N-C | 232 | 20 | [7] |
| Mn _{0.73} Ru _{0.27} O _{2-d} | 208 | 10 | [8] |
| PtCo-RuO ₂ /C | 212.6 | 20 | [9] |
| FeCoNiIrRu/CNFs | 241 | 20 | [10] |
| RuCoO _x | 200 | 100 | [11] |
| Nd _{0.1} RuO _x /CC | 211 | 25 | [12] |
| Ru _{0.6} W _{17.4} O _{49-δ} | 252 | 45 | [13] |
| Ru _{0.85} Zn _{0.15} O _{2-δ} | 190 | 50 | [14] |
| SS Pt-RuO ₂ HNSs | 228 | 100 | [15] |

Table S3 The concentrations of dissolved Ru and Ce cations in the electrolyte during OER time were determined by ICP-MS.

| C(catalyst) \ Time | 50 h | 100 h | 150 h | 200 h |
|---|----------|-----------|----------|----------|
| $C_{\text{Ru}}(\text{Ce}_{0.05}\text{Ru}_{0.95}\text{O}_2)$ | 4.35 ppb | 6.54 ppb | 7.56 ppb | 8.82 ppb |
| $C_{\text{Ru}}(\text{RuO}_2)$ | 9.68 ppb | 17.23 ppb | | |
| $C_{\text{Ce}}(\text{Ce}_{0.05}\text{Ru}_{0.95}\text{O}_2)$ | 0.02 ppb | 0.03 ppb | 0.03 ppb | 0.04 ppb |

Reference

- [1] Delley, B., An all-electron numerical method for solving the local density functional for polyatomic molecules. *The Journal of Chemical Physics* **1990**, *92* (1), 508-517.
- [2] Delley, B., From molecules to solids with the DMol3 approach. *The Journal of Chemical Physics* **2000**, *113* (18), 7756-7764.
- [3] Perdew, J. P.; Burke, K.; Ernzerhof, M., Generalized Gradient Approximation Made Simple. *Physical Review Letters* **1996**, *77* (18), 3865-3868.
- [4] Rossmeisl, J.; Logadottir, A.; Nørskov, J. K., Electrolysis of water on (oxidized) metal surfaces. *Chemical Physics* **2005**, *319* (1), 178-184.
- [5] Nørskov, J. K.; Rossmeisl, J.; Logadottir, A.; Lindqvist, L.; Kitchin, J. R.; Bligaard, T.; Jónsson, H., Origin of the Overpotential for Oxygen Reduction at a Fuel-Cell Cathode. *The Journal of Physical Chemistry B* **2004**, *108* (46), 17886-17892.
- [6] Wang J, Cheng C, Yuan Q, et al. Exceptionally active and stable RuO₂ with interstitial carbon for water oxidation in acid [J]. *Chem*, 2022, 8(6): 1673-87.
- [7] Rong C, Shen X, Wang Y, et al. Electronic structure engineering of single-atom Ru sites via Co–N₄ sites for bifunctional pH-universal water splitting [J]. *Advanced Materials*, 2022, 34(21): 2110103.
- [8] Wang K, Wang Y, Yang B, et al. Highly active ruthenium sites stabilized by modulating electron-feeding for sustainable acidic oxygen-evolution electrocatalysis [J]. *Energy & Environmental Science*, 2022, 15(6): 2356-65.
- [9] Yang J, Li M, Sun Z, et al. Prolonging the cycling lifetime of lithium metal batteries with a monolithic and inorganic-rich solid electrolyte interphase [J]. *Energy & Environmental Science*, 2023, 16(9): 3837-46.
- [10] Zhu H, Zhu Z, Hao J, et al. High-entropy alloy stabilized active Ir for highly efficient acidic oxygen evolution [J]. *Chemical Engineering Journal*, 2022, 431: 133251.
- [11] Zhu W, Yao F, Cheng K, et al. Direct Dioxygen Radical Coupling Driven by Octahedral Ruthenium–Oxygen–Cobalt Collaborative Coordination for Acidic Oxygen

Evolution Reaction [J]. *Journal of the American Chemical Society*, 2023, 145(32): 17995-8006.

[12] Li L, Zhang G, Xu J, et al. Optimizing the electronic structure of ruthenium oxide by neodymium doping for enhanced acidic oxygen evolution catalysis [J]. *Advanced Functional Materials*, 2023, 33(10): 2213304.

[13] Wang X, Jang H, Liu S, et al. Enhancing the catalytic kinetics and stability of Ru sites for acidic water oxidation by forming Brønsted acid sites in tungsten oxide matrix [J]. *Advanced Energy Materials*, 2023, 13(36): 2301673.

[14] Hou L, Li Z, Jang H, et al. Electronic and lattice engineering of ruthenium oxide towards highly active and stable water splitting [J]. *Advanced Energy Materials*, 2023, 13(22): 2300177.

[15] Wang J, Yang H, Li F, et al. Single-site Pt-doped RuO₂ hollow nanospheres with interstitial C for high-performance acidic overall water splitting [J]. *Science advances*, 2022, 8(9): eabl9271.